FTIR Imaging of Polymer Dissolution. 2. Solvent/Nonsolvent Mixtures

Travis Ribar and Jack L. Koenig*

Department of Macromolecular Science, Case Western Reserve University, Cleveland, Ohio 44106

Rohit Bhargava

Laboratory of Chemical Physics, NIDDK, National Institutes of Health, Bethesda, Maryland 20892

Received July 5, 2001; Revised Manuscript Received August 28, 2001

ABSTRACT: Fourier transform infrared (FTIR) spectroscopic imaging employing focal plane array (FPA) detection is used to study the dissolution of poly(α-methylstyrene) (PAMS) by solvent solutions containing systematically varied amounts of a nonsolvent. Sequential images were acquired as dissolution proceeded and the samples were not disturbed during image acquisition. Qualitative spatial and chemical distribution of each species within the field of view was obtained by analyzing images based on the characteristic vibrational modes of each species, while quantitative information was gathered through the calculation of individual concentration profiles along the chemical gradient. The images and absorbance profiles showed selective solvent penetration in all cases. In general, the dissolution rate of the polymer decreased linearly with the weight-percent of nonsolvent present in the solution. Anomalously high dissolution rates were observed for solutions containing ∼5−10% nonsolvent. This increase was attributed to the formation of a band of high polymer concentration perpendicular to solvent diffusion direction during the dissolution process. The efficacy of FTIR imaging in studying the spatiotemporal variation of microscopic gradient evolution in multicomponent systems is underscored.

Introduction

Polymer dissolution is an important aspect of many everyday applications and cutting-edge technologies, ranging from sophisticated microelectronic fabrication to temporally controlled drug delivery applications.[1−5] However, the exact physical mechanisms behind dissolution are not fully understood, partly due to the lack of analytical techniques capable of providing both spatial and chemical information on a microscopic scale. Numerous physical models have been proposed to predict the behavior of a polymer dissolving in a solvent,[6−8] but studies on the dissolution of a polymer by a solvent mixture are less common.[9] The complexities of such a system prevent a simple generalized mathematical or physical model from being constructed. Even in cases where such attempts have been made, the inability to monitor the process experimentally in a manner such that information both on the dissolution process and on the individual components in the system may be recorded prevents further development. Spatially resolved and chemically specific data regarding the dissolution of a polymer in a solvent have been measured using techniques ranging from simple blot-and-weigh methods to complex analytical techniques providing specific (though often not enough) information. For example, NMR,[10] polar ellipsometry,[11,12] FTIR spectroscopy,[13−15] ATR spectroscopy,[13,16,17] and Rutherford backscattering spectroscopy[18] yield chemically and/or spatially sensitive data based on optical or magnetic properties but may not be able to provide *both* the highly specific chemical information and the spatial selectivity needed to properly characterize complex dissolution processes.

Chemical imaging techniques allow for such data to be collected directly. Magnetic resonance imaging (MRI) has been used to characterize polymer dissolution,[19,20] but the spatial resolution of these experiments is close to a fraction of a millimeter, experimental times are long, and fast diffusion phenomena may not be examinable. Other imaging techniques that include microscopy,[21] refractive index measurements,[22] and radiation detection due to labeling[23] are chemically nonspecific unless labeling is carried out, which may change the transport properties of the system. The recent coupling of a focal plane array detector to an interferometer[24] has given us the capability to rapidly image large fields of view at a high spatial resolution. A field of view spanning hundreds of microns may be imaged in less than 5 min with spatial resolutions approaching the IR radiation wavelength diffraction limit. The well-known chemical specificity of infrared spectroscopy is preserved in an imaging modality, providing for a convenient tool to characterize certain diffusion behaviors that are intractable by other means.

FTIR imaging has been applied to study multicomponent polymer systems[25] ranging from semicrystalline polymers,[26] to polymer-liquid crystal composites,[27,28] to diffusion processes.[29−31] The dissolution of a polymer by a solvent mixture containing two known solvents for a polymer has been previously monitored using FTIR imaging.[32] The aim of the study reported in this manuscript is to observe the dissolution of a polymer in a solvent mixture containing a known solvent in a known nonsolvent by this new FTIR imaging technique. While the behavior of such systems has been the subject of theoretical and experimental curiosity,[33,34] the application of FTIR imaging allows for an experimental examination of microscopic chemical gradients of all involved components as a function of time.

Experimental Section

The polymer used in this study, poly(α-methylstyrene) [PAMS] (M_w = 4000; T_g ∼ 79 °C), was obtained from Aldrich Chemical. Methyl isobutyl ketone (MIBK, obtained from Fisher Scientific) and deuterated methanol (CD_3OD, 99.5

* To whom correspondence should be addressed.

10.1021/ma011152x CCC: $20.00
Published on Web 10/06/2001

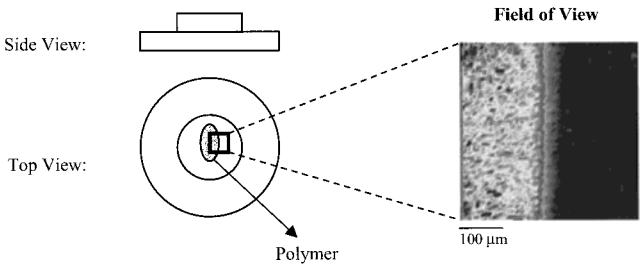

Figure 1. Graphical representation of the samples used here. The image used to represent the field of view reflects the absorbance of the polymer at the onset of dissolution by a solvent mixture containing 20% by weight nonsolvent.

atom % deuterated; obtained from Aldrich) were the low molecular weight penetrants used in the experiment. MIBK and CD_3OD are solvent and nonsolvent, respectively, for the polymer and will be referred to as such throughout this paper. All materials were used as received without further purification. Weight ratios of the nonsolvent in the solvent were measured and a liquid solution was made prior to diffusion. To be concise, these mixtures are referred to as solutions in the paper and all reports of a certain solution are referenced by the weight fraction of the nonsolvent.

Experiments were conducted using the contact method.[35] To prepare a thin layer of polymer sandwiched between two salt plates, a small granule of solid polymer was placed on 2 mm thick CaF_2 substrates and was heated on a hot stage to 150 °C. A substrate was then placed on top of the polymer granule, and the two plates were clamped together. The sample was placed in an oven at 150 °C for 3 h, after which it was allowed to cool in ambient air to room temperature. The clamps were removed to yield a polymer film partially occupying space between the two salt plates. A graphical representation of a sample prepared by this method is shown in Figure 1. In all cases, the film created was wide enough that the area imaged was not affected by dissolution occurring outside the field of view. A solution was introduced from one end after the sample was positioned in the spectrometer. The solution entered the space between the substrates due to capillary action and came into contact with the polymer, thus initiating the dissolution process. Images were sequentially acquired during the time it took the solvent mixture to completely dissolve the polymer from the field of view. Solution was added to the setup to compensate for evaporation as necessary. This evaporation did not affect the composition of the solvent in the setup, as can be readily confirmed by time-resolved spectra of the solvent mixture.

Infrared images were acquired using the Bio-Rad Stingray imaging spectrometer.[36] The Stingray is comprised of an FTS 6000 step-scan interferometer bench coupled to a microscope accessory, UMA-500. The imaging detector used here is a Santa Barbara focal plane FPA consisting of a 64 × 64 array of mercury cadmium telluride (MCT) elements imaging an average spatial area of 400 μm × 400 μm. A long pass filter to eliminate unwanted wavelengths and prevent Fourier fold-over perturbations was inserted into the beam path. An 8 cm^{-1} nominal spectral resolution and an undersampling ratio (UDR) of 4 were used for the study. A mirror stepping rate of 5 Hz (200 ms/step) was used, yielding a total scanning time of about 210 s. The number of camera frames (frame rate = 252 Hz) averaged during each spectrometer step was 16. Image processing and data extraction were carried out using the hyperspectral imaging software package Environment for Visualizing Images (ENVI) (Research Systems Inc.) Lower noise absorbance profiles were extracted from each image by within-image co-addition[30] of spectral data from a forty micrometer region of the image perpendicular to the diffusion direction.

Results and Discussion

The presence of individual components in the diffusion process can be monitored using their characteristic infrared absorbance peaks. Absorbance spectra of the polymer and each solvent used are seen in Figure 2. The polymer was monitored using the peak at 1600 cm^{-1}, which is due to its phenyl ring quadrant stretching mode of vibration. MIBK was characterized using the peak at 1172 cm^{-1} (CCC asymmetric stretching mode) and CD_3OD was measured using the peak at 2066 cm^{-1} (C−D stretching mode). Chemically specific images for each component within the system were obtained by plotting the intensity of a characteristic IR peak in each pixel of the FPA scaled to the values shown in the corresponding color bars (Figure 3). A complete set of images taken during a single dissolution experiment (Figure 3) shows the gradual dissolution of the polymer and ingress of each solvent typically seen (except at some concentrations, vide infra). In this manner, a single experiment yields both spatial and chemical data on each component within the system, eliminating the need to perform numerous experiments to characterize the behavior of each component. To calculate an absorbance profile for any substance in the system, the intensity of its characteristic IR peak along the diffusion direction can be extracted. As the distance between the sandwiched substrates does not change, the thickness of the polymer layer is constant (as determined by imaging before starting the experiment) and specific interactions (if any) are not expected to affect the selected modes of vibration, Beer's law dictates that the concentration change is proportional to the absorbance change. For this reason, the terms absorbance profile and concentration profile are used synonymously within this paper. This relationship is discussed in more detail elsewhere.[32]

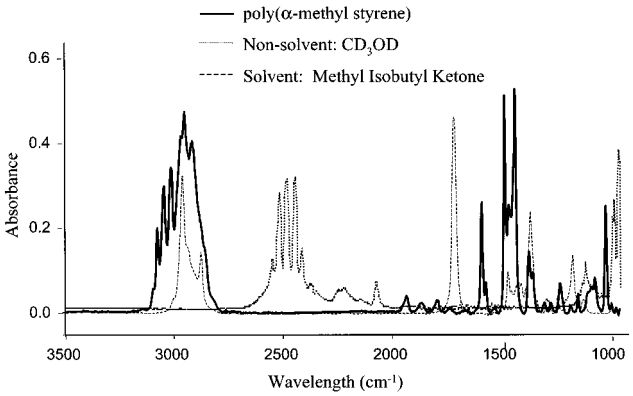

Figure 2. Infrared spectra of system components.

While the distribution of each component can be visualized by images, as shown in Figure 3, the extraction of a diffusion profile is useful in monitoring the concentration distribution. Figure 4a shows an absorbance image of PAMS after 11 min of dissolution in a solvent/nonsolvent system containing 20% by weight nonsolvent. The absorbance profiles of each component in the image are shown in Figure 4b. To compare distributions across samples and concentrations, the absorbance of a species is normalized (scaled from 0 to 1) using each material's maximum absorbance in the image (at 100% solvent solution concentration for each of the penetrants and at 100% polymer concentration for the polymer). In Figure 4b, it is seen that MIBK has preferentially penetrated the polymer even at this (early) stage of polymer dissolution. The concentration profiles of the solvents demonstrate that the diffusion front is sharper for the nonsolvent as compared

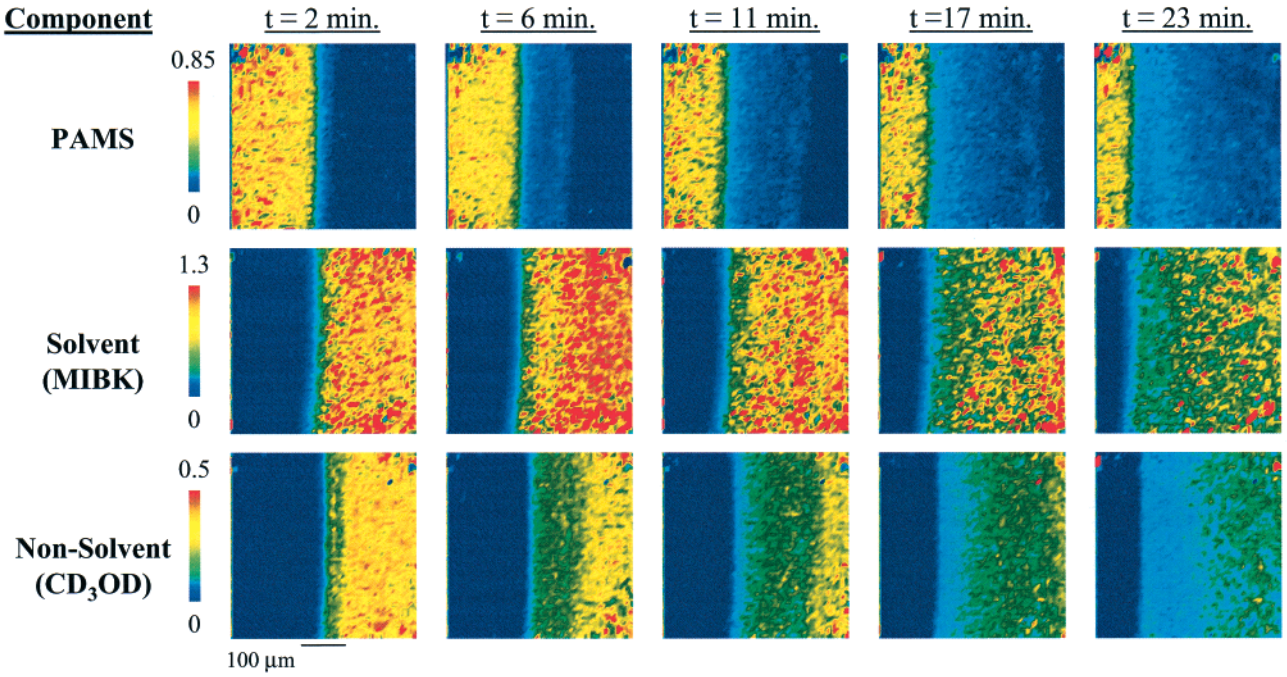

Figure 3. Images acquired during dissolution of a polymer by a solvent mixture containing 15 wt % nonsolvent. Images reflect the absorbance of the substance listed to their left and are scaled to the corresponding color bar values indicated next to the name on the left. The elapsed time after initial contact between polymer and solvent that the image represents is listed above each column of images.

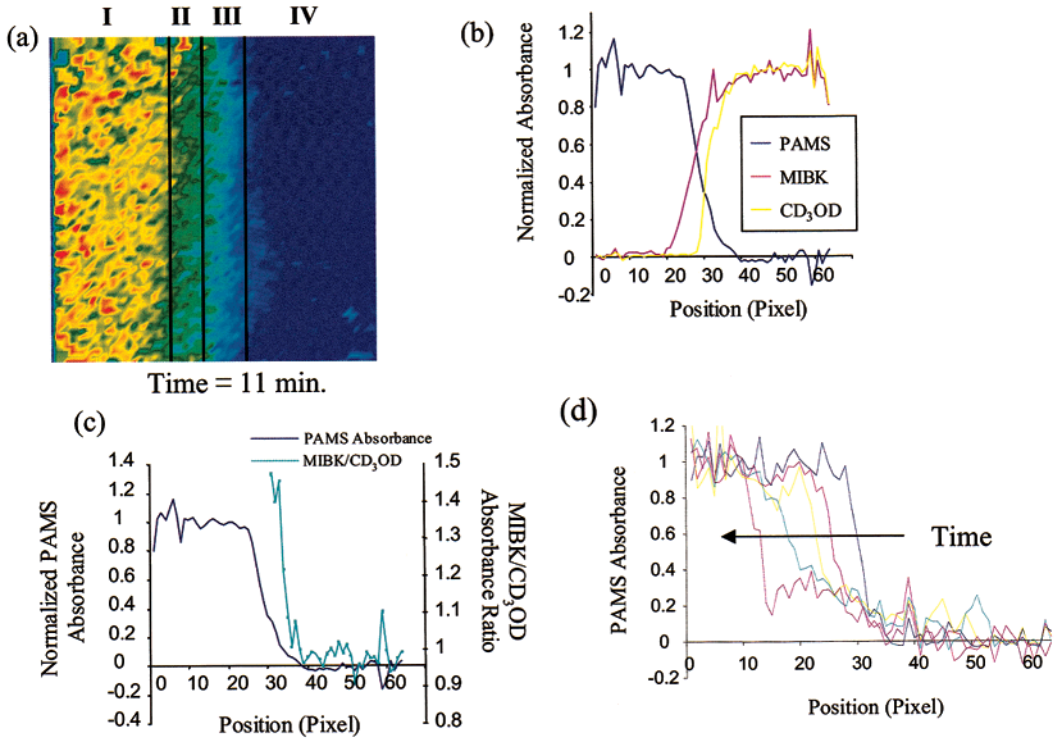

Figure 4. (a) An IR image reflecting the absorbance of the polymer during dissolution in a solvent solution containing 20% by weight nonsolvent. The image has been separated into regions typically seen during dissolution: (I) the bulk polymer; (II) polymer selectively penetrated by solvent; (III) dissolved chain layer; (IV) bulk solvent. (b) Corresponding absorbance profiles for each element in the image. Values are scaled from 0 to 1. (c) Normalized absorbance of the polymer and the solvent ratio plotted as a function of position. (d) Time evolution of the concentration profile of the polymer.

to the solvent. This result was common to all solvent systems.

The relative composition of the solvent solution at any given position is indicated by the ratio of the absorbance of the normalized solvent-specific peak to the normalized nonsolvent-specific peak. A change in this ratio reflects a corresponding change in the relative concentration of solvent to nonsolvent in the solvent solution. Figure 4c shows the value of this ratio superimposed on the absorbance profile of the polymer. It is seen that this ratio starts to increase as the original polymer/solvent mixture interface is approached and rapidly

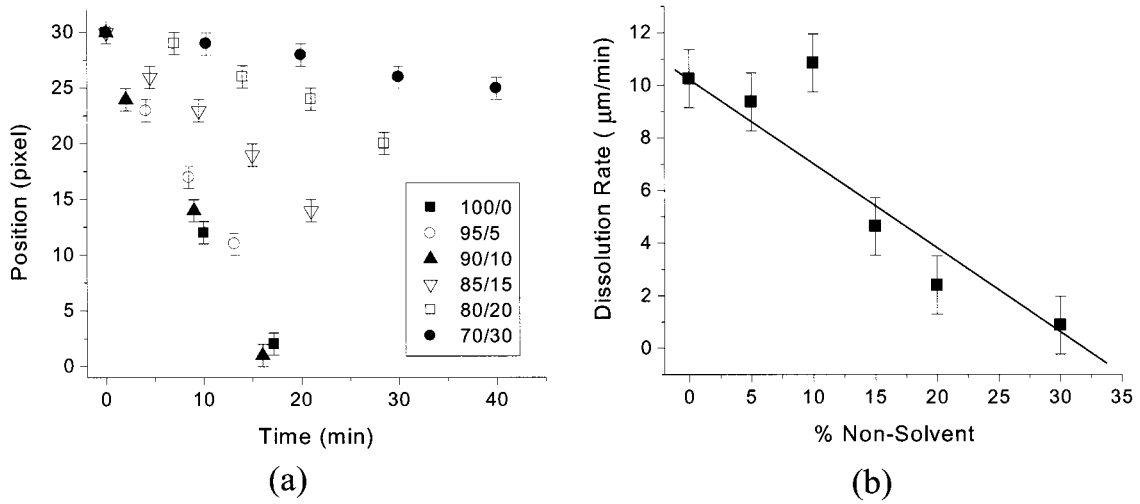

Figure 5. (a) Polymer/solvent interface position plotted against time for all solvent systems. The relationship in all cases is linear. (b) Dissolution rate of the polymer as a function of solvent composition. The relationship is linear, with the exception of when the solvent solution contains 10% nonsolvent.

rises as the polymer bulk is approached. This is a result of the selective penetration of solvent (as opposed to nonsolvent) into the polymer. Clearly, the ratio is meaningless in the polymer bulk and is therefore not plotted. The ratio starts to diverge rapidly due to the combination of the concentration of the nonsolvent approaching zero and the concentration of solvent remaining relatively high and is thus plotted to within ~15 μm of the bulk polymer.

Analysis of Figure 4, parts b and c, shows that the penetrant in the polymer region closest to the bulk consists of only the solvent. It appears that the nonsolvent is therefore completely excluded from the initiation of the dissolution process. It is interesting to note that the preferential ingress of the solvent should leave an excess of the nonsolvent in the layers immediately following the selectively penetrated layer. However, we see the absence of such a gradient, probably due to the orders of magnitude faster diffusion of the components within the bulk solvent mixture and the relatively large pool of solvent mixture as compared to the thin layer of selective penetration.

Concentration profiles in these experiments show the evolution of a complex system during dissolution. Figure 4a is divided into four distinct regions that are observed at the polymer/solvent mixture interface during typical dissolution of the polymer. These regions are defined both by polymer concentration and by the extent of solvent and nonsolvent penetration. The first region (region I) is the bulk polymer that has not been penetrated by the solvent solution. Proceeding from left to right across the image, this region is followed by a region of polymer that has been selectively penetrated by only the solvent, and the nonsolvent is completely excluded (region II). Dissolved polymer is present in this region and the next (region III), where nonsolvent is present, but at a concentration lower than that of the bulk solvent solution. The furthest region (IV) from the bulk polymer consists of the bulk solution, into which no polymer has yet dissolved.

The dissolution rates of each system were measured from time-resolved absorbance profiles of the polymer (Figure 4d). The polymer/solvent interface was plotted as a function of time to determine the rate of dissolution. The interface-vs-time graphs at each solvent composition (shown in Figure 5a) have good linear fits, and the dissolution rates appear to be constant in each experiment over the area imaged, leading to speculation that the polymer dissolution rate is determined only by the penetration of the solvent. The polymer dissolution rate is shown in Figure 5b as a function of weight percent nonsolvent present in the solvent solution. The dissolution rate of the polymer varies linearly with solvent composition, with the notable exception of when the solvent solution contains 10% by weight nonsolvent. That case presents a unique phenomenon that is discussed next.

Dissolution in a system where the solvent mixture consists of 10% by weight nonsolvent shows behavior different from the other solvent solution compositions measured, as shown in Figure 6. These images are similar to those representative of the dissolution process at other solution compositions (Figure 3). However, as Figure 5b demonstrates, the dissolution rate of the polymer at 10 wt % nonsolvent not only is higher than the linear relationship suggested by the other dissolution rates obtained but is also higher than the dissolution rate of the polymer in the pure solvent! To understand this phenomenologically, the concentration distribution of each species is visualized (Figure 6).

A major feature unique to dissolution at this solvent composition is the evolution of a second polymer interface. The band of abnormally high polymer concentration moves as a single unit away from the bulk polymer—not as a diffusive interphase as observed at higher solution compositions. Though the time scale on which measurements are taken does not allow for a complete observation of the formation of this layer before it starts to move from the bulk polymer, images do show a gradual separation of this layer from the polymer bulk over the course of the experiment.

An examination of the concentration profiles of the polymer (Figure 7a) reveals the second interface to be a region of relatively high polymer concentration. The time-resolved profiles also display the movement of the interface within the field of view. Using the methods used earlier, an image containing the polymer dissolving in the presence of a second interface may be divided into characteristic regions and are done so in Figure 7b. Regions I, II, III, and IV correlate to the regions

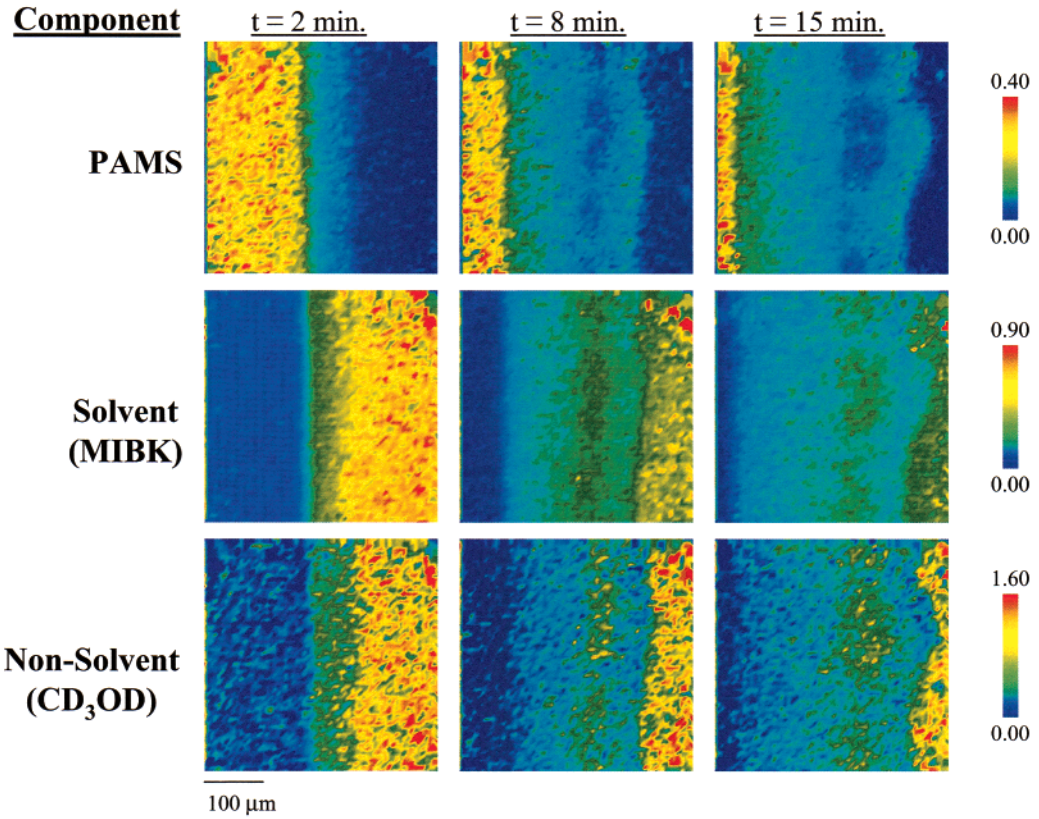

Figure 6. Images taken during dissolution in a solvent mixture containing 10 wt % nonsolvent. Images reflect the absorbance of the substance listed to their left and are scaled to the color bar values on the right. The elapsed time after initial contact between polymer and solvent that the image represents is shown above each column of images.

observed in dissolution without the second interface (Figure 4a) and represent the bulk polymer, a thin layer of exclusive solvent penetration, the solvent-rich dissolved layer, and the bulk mixture, respectively. The polymer and solvent behaviors within these regions are as discussed previously. The additional region, region V in the figure, is the second interface. This interface is marked by an increase in both the polymer concentration and the relative concentration of solvent in the solvent solution, as indicated by solvent/nonsolvent ratio calculations (Figure 7c). The solvent/nonsolvent ratio, which was previously constant until reaching the layer closest to that of solvent penetration, now displays an increasing solvent concentration leading from the secondary interface toward the polymer bulk. We believe that this is a direct consequence of the inability of both the solvent and the nonsolvent to undergo fast diffusion across the secondary front. Thus, a simple mass balance in the confined volume of the mixture between the second interface and the bulk and the selective solvent penetration into the polymer leads to the gradient present in Figure 7c. Hence, a decreasing solvent/nonsolvent ratio is observed between the bulk polymer and the second interface.

As expected, individual concentration profiles for the solvent and nonsolvent (Figure 7d) are also markedly different compared to other cases, reflecting the phenomenon discussed above. The mechanism behind the formation of the secondary interface is not clear. There are two possible explanations: stress−cracking or dissolution−condensation. Stress−cracking has been observed in many glassy polymers and the microscopic appearance of the phenomenon is well-analyzed.[37] A distinct feature of stress−cracking induced dissolution is the complete absence of a gel layer. Such behavior has been observed for higher polymers,[38] and a clear absence of a gel layer can be seen here. Further, stress cracking does not stop after an initial layer but rather is a continual process. To determine whether that is the case here, a sample containing the polymer dissolving in a solution containing 10% by weight nonsolvent is moved such that the bulk polymer interface remains in the field of view. This allows us to observe the interface for a longer period of time. Figure 8 shows the images taken under these conditions. The figure shows that after the formation of the first secondary front, diffusion of the solution into the polymer proceeds as it does with other solution concentrations. The secondary interface, once formed, is fairly uniform in position, width, and appearance over time—as opposed to what stress−cracking-induced breaking from the polymer bulk would entail. Stress−cracking-assisted dissolution is therefore not present in this system.

As observed previously, the solvent preferentially diffuses into the polymer, leaving behind a nonsolvent rich gradient that is quickly neutralized by the bulk solution. This is used to explain the anomalous dissolution behavior seen here. When only small amounts of nonsolvent are present in the solvent solution, the absolute difference in concentration of the nonsolvent induced by the preferential ingress of the solvent is insufficient to provide a strong driving force for neutralization of this gradient. Before the nonsolvent composition can be equilibrated with the bulk solution, the polymer dissolved by the solvent reaches the layer of high nonsolvent composition, causing the polymer to condense and expel the nonsolvent toward the bulk. This dissolution−condensation mechanism is the

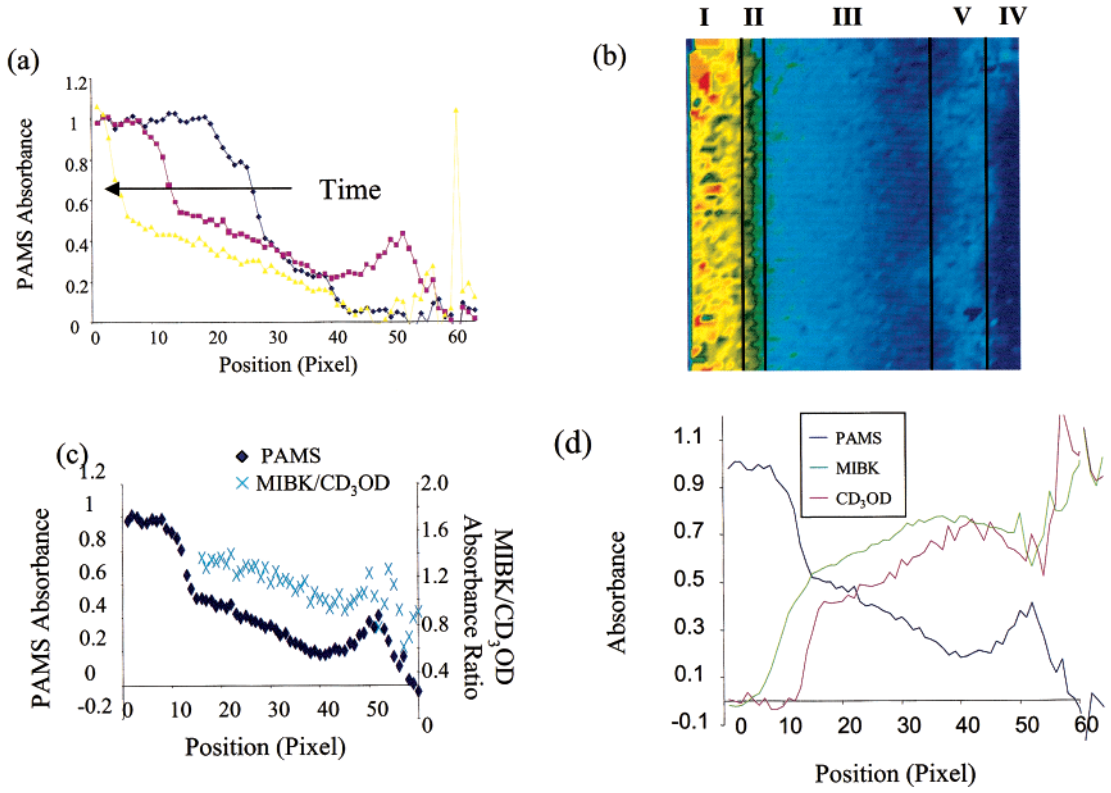

Figure 7. (a) Time evolution of the concentration profile of the polymer. (b) Corresponding absorbance profiles for each element in the image. Values are scaled from 0 to 1. (c) Normalized absorbance of the polymer and the solvent ratio plotted as a function of position. (d) Regions in an image containing a second interface. Key: (I) the bulk polymer; (II) polymer selectively penetrated by solvent; (III) dissolved chain layer; (IV) bulk solvent; (V) second interface. The image shown represents the absorbance of PAMS.

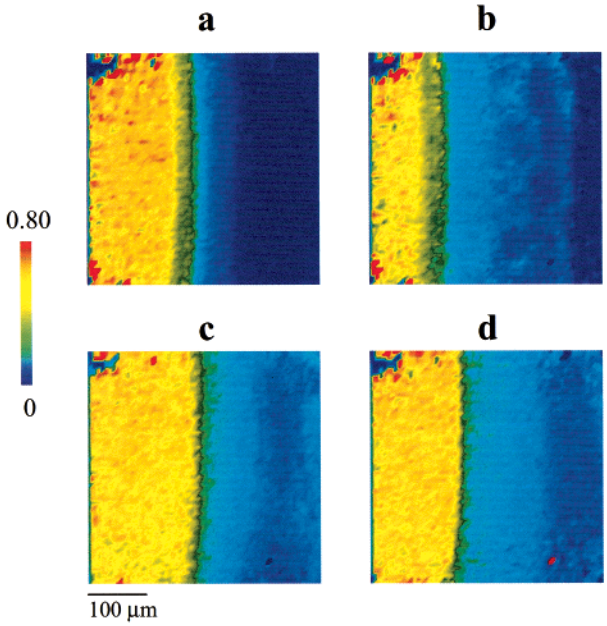

Figure 8. Moving sample to view the interface. a and b represent images taken at the initial sample position. After the image represented by b was taken, the sample was moved to re-center the polymer/solvent interface. Images c and d were taken at the second position. The second interface is seen in b. Key: (a) taken 2 min after solvent contact; (b) taken 8 min after contact; (c) taken 15 min after contact; (d) taken 22 min after contact. All images represent the absorbance of PAMS and are scaled to the values on the color bar to the left.

most probable mechanism given the evidence at hand. Further, for a 5% nonsolvent concentration, a similar secondary interface is observed while for 15% nonsolvent it is not. Hence, there appears to be a critical 10−12% concentration of the nonsolvent that mitigates concentration dictated driving forces for diffusion to the extent that the dynamics of solvent dissolution and condensation are faster than even solvent/non- solvent diffusion. To capture the essence of the formation of the secondary front, faster imaging methods need to be employed. Efforts to implement such methods are discussed elsewhere.[39]

Conclusions

FT-IR imaging was successfully used to monitor the early stages of dissolution of a glassy polymer in a solvent mixture containing systematically varied amounts of nonsolvent. Real-time information on the behavior of each component in the system was obtained without disturbing the diffusion processes and quantitative information was gathered through the calculation of corresponding absorbance profiles. In this system, a selective penetration of the polymer by the solvent was observed in cases, conclusively demonstrating that when a polymer is subject to solvents of varying quality, solvent fractionation takes place and the ingress of mixture is facililated by the preferential ingress of the solvent of superior quality. The dissolution rate of the polymer was found to have a linear relationship to the weight-percent nonsolvent present in the solvent solution with the exception of when the solvent solution contained small amounts (by weight) of nonsolvent. The increase in the dissolution rate of this system to a level above the measured rate in pure solvent was attributed to the formation of a second polymer interface, leading us to believe that localized polymer and solvent con-

centration dynamics play a decisive role in the dissolution of polymers.

Acknowledgment. This work is financially supported in part by the National Science Foundation Center for Advanced Liquid Crystalline Optical Materials (ALCOM).

References and Notes

(1) Heller, J.; Baker, R. W.; Gale, R. M.; Rodin, J. O. *J. Appl. Polym. Sci.* **1978**, *22*, 1991.
(2) Lee, P. I. *J. Controlled Release* **1985**, *2*, 277.
(3) Korsmeyer, R. W.; Lustig, S. R.; Peppas, N. A. *J. Polym. Sci., Polym. Phys. Ed.* **1986**, *24*, 395.
(4) Papanu, J. S.; Hess, D. W.; Soane, D. S.; Bell, A. T. *J Appl. Polym. Sci.* **1990**, *39*, 803.
(5) Narasimhan, B.; Peppas, N. A. *Adv. Polym. Sci.* **1997**, *128*, 157−207.
(6) Tu, Y. O.; Ouano, A. C. *IBM J. Res. Dev.* **1977**, *21*, 131−142.
(7) Devotta, I.; Badiger, M. V.; Rajamohanan, P. R.; Ganapathy, S.; Mashelkar, R. A. *Chem. Eng. Sci.* **1995**, *55*, 2557−2569.
(8) Narasimhan, G.; Peppas, N. A. *J. Polym. Sci., Polym. Phys. Ed.* **1996**, *34*, 947−961.
(9) Devotta, I.; Mashelkar, R. A. *Chem. Eng. Commun.* **1996**, *156*, 31−43.
(10) Bastow, T. J.; Hodge, R. M.; Hill, A. J. *J. Membr. Sci.* **1997**, *131*, 207.
(11) Papanu, J. S.; Hess, D. W.; Bell, A. T.; Soane, D. S. *J. Electrochem. Soc.* **1989**, *136*, 1195.
(12) Papanu, J. S.; Hess, D. W.; Soane, D. S.; Bell, A. T. *J. Appl. Polym Sci.* **1990**, *39*, 803.
(13) Schlotter, N. E.; Furlan, P. Y. *Vibr. Spectrosc.***1992**, *3*, 147.
(14) Van Alsten, J. G.; Lustig, S. R. *Macromolecules* **1992**, *25*, 5069.
(15) Jabbari, E.; Peppas, N. A. *Macromolecules* **1993**, *26*, 2175.
(16) Fieldson, G. T.; Barbari, T. A. *Polymer* **1993**, *34*, 1146.
(17) Fieldson, G. T.; Barbari, T. A. *AIChE J.* **1995**, *41*, 795.
(18) Mills, P. J.; Palmstrom, C. J.; Kramer, E. J. *J. Mater. Sci.* **1986**, *21*, 1479.
(19) Weisenberger, L. A.; Koenig, J. L. *Appl. Spectrosc.* **1989**, *43*, 1117.
(20) Grinsted, R. A.; Clark, L.; Koenig, J. L. *Macromolecules* **1992**, *25*, 1235.
(21) Thomas, N. L.; Windle, A. H. *Polymer*, **18** 1977 1195.
(22) Crank, J.; Robinson, C. *Proc. R. Soc. London A* **1950**, *204*, 339.
(23) Bueche, F.; Cashin, W. M.; Debye, P. V. *J. Chem. Phys.* **1952**, *20*, 1956.
(24) Lewis, E. N.; Treado, P. J.; Reeder, R. C.; Story, G. M.; Dowrey, A. E.; Marcott, C.; Levin, I. W. *Anal. Chem.* **1995**, *67*, 3377.
(25) Koenig, J. L.; Wang, S. Q.; Bhargava, R. *Anal. Chem.*, in press.
(26) Snively, C. M.; Koenig, J. L. *J. Polym. Sci. B* **1999**, *37*, 2353.
(27) Bhargava, R.; Wang, S. Q.; Koenig, J. L. *Appl. Spectrosc.* **1998**, *52*, 323.
(28) Bhargava, R.; Wang, S. Q.; Koenig, J. L. *Macromolecules* **1999**, *32*, 2748.
(29) Snively, C. M.; Koenig, J. L. *Macromolecules* **1998**, *31*, 3753.
(30) Bhargava, R.; Ribar, T.; Koenig, J. L. *Appl. Spectrosc.* **1999**, *53*, 1313.
(31) Snively, C. M.; Koenig, J. L. *J. Polym. Sci. B* **1999**, *37*, 2261.
(32) Ribar, T.; Bhargava, R.; Koenig, J. L. *Macromolecules* **2000**, *33*, 8842.
(33) Pethrick, R. A.; Rankin, K. E. *J. Mater. Chem.* **1998**, *8*, 2591.
(34) Rankin, K. E.; Pethrick, R. A. *Microelectron. Eng.* **1995**, *26*, 141.
(35) Challa, S. R.; Wang, S. Q.; Koenig, J. L. *Appl. Spectrosc.* **1996**, *50*, 1339.
(36) *Bio-Rad*; Digilab Laboratories: Cambridge, MA.
(37) Ueberreiter, K. In *Diffusion in Polymers*; Crank, J., Park, J. G., Eds.; Academic Press: London, 1968; pp 220−258.
(38) Koenig, J. L.; Wang, S. Q.; Bhargava, R. *Anal.Chem.*, in press.
(39) Ribar, T.; Koenig, J. L.; Bhargava, R. Manuscript under preparation.

MA011152X